Electronic Supplementary Material (ESI) for New Journal of Chemistry.

Supporting Information

Fabrication of core-shell AuNP@UIO-66/Au nanoparticles for *in situ* SERS monitoring the degradation process

Zhou-Ya Wu[a], Meng-Meng Zhang[a], Yuan-Yuan Yang[b], Sheng Han[a*], Yuan-Ting Li[a*]

[a] School of Chemical and Environmental Engineering, Shanghai Institute of Technology, Shanghai 201418, P. R. China

[b] College of Environmental Science & Engineering, Tongji University, 1239 Siping Road, Shanghai 200092, China

*Corresponding author:

Sheng Han; Yuan-Ting Li

School of Chemical and Environmental Engineering

Shanghai Institute of Technology

No. 100 Haiquan Road

Shanghai, 201418, P. R. China

Tel/Fax: + 086 21 60873241

E-mail: hansheng654321@sina.com (S. Han); joice319@hotmail.com (Y.T. Li)

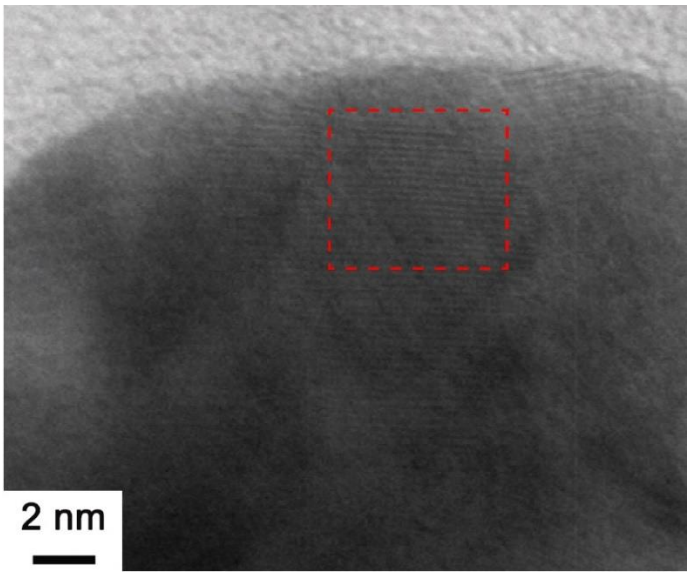

Fig. S1. HRTEM images of core-shell AuNP@UIO-66 nanoparticles.

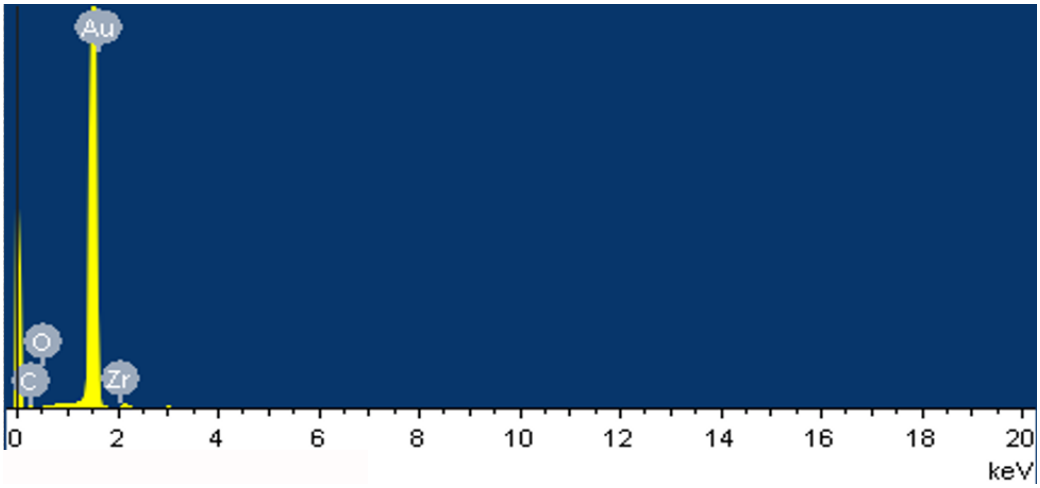

Fig. S2. EDS spectrum of Au@UIO-66/Au nanoparticles.

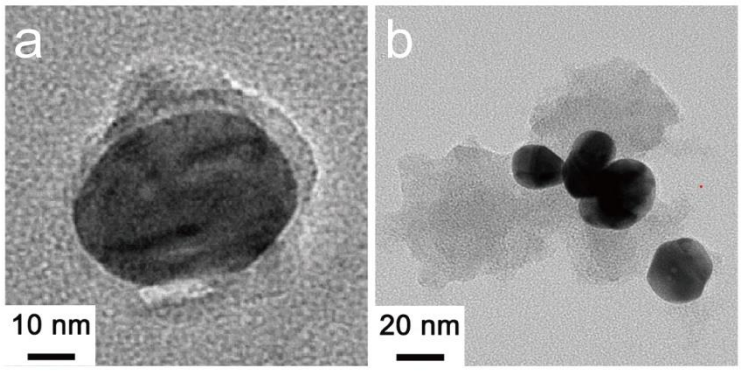

Fig. S3. TEM images of AuNP@UIO-66 nanoparticles fabricated with different volume ratio of $HAuCl_4$ to MOF precursor solution (a) 35:1 and (b) 10:1.

Fig. S4. Image of AuNP@PVP colloidal solution.

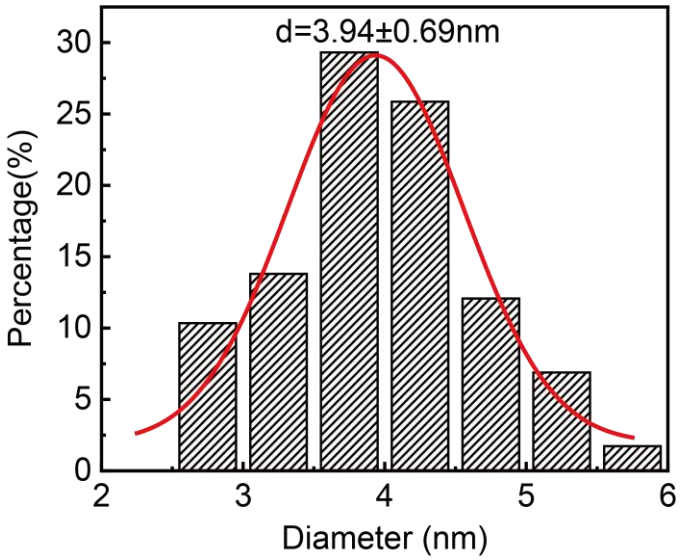

Fig. S5. The size distribution of AuNPs loading on the surface of AuNP@UIO-66.

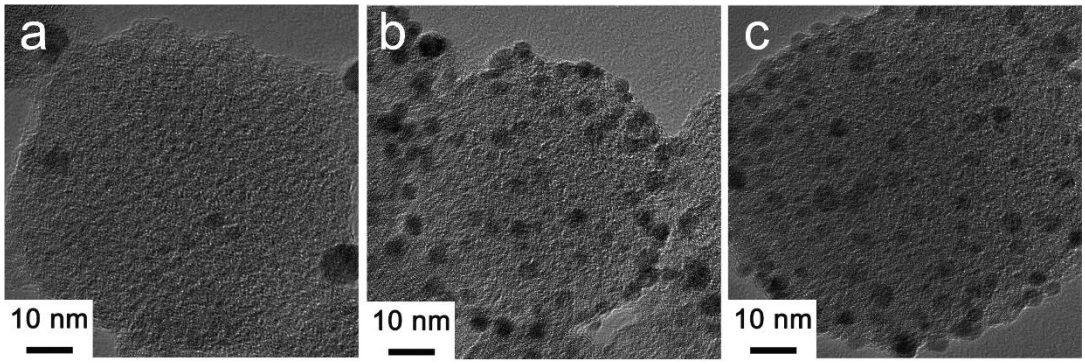

Fig. S6. TEM images of AuNP@UIO-66/Au after loading with 4 nm AuNPs at the reaction time (a) 6 h, (b) 12 h and (c) 24 h.

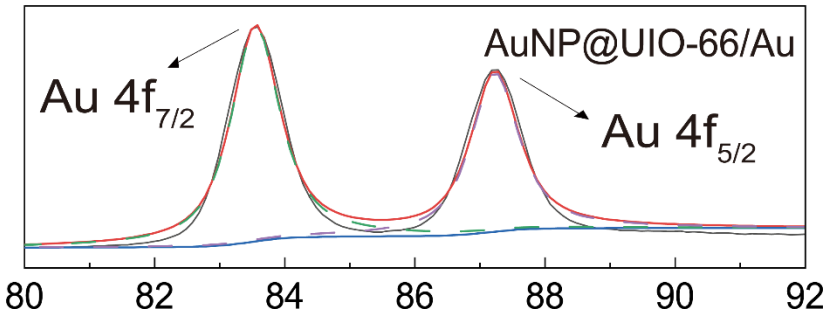

Fig. S7. XPS spectra for Au 4f of AuNP@UIO-66/Au.

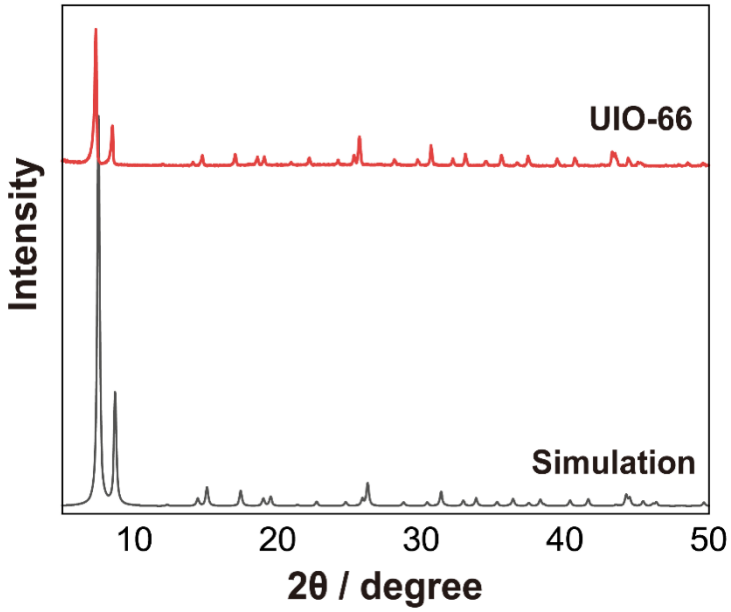

Fig. S8. The XRD pattern of the as-prepared UIO-66 powder and the simulation pattern.

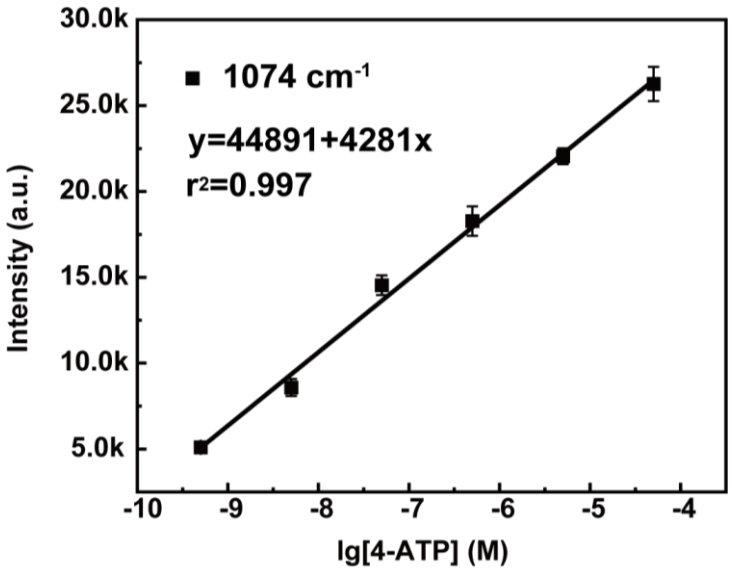

Fig. S9. The linear relationship of SERS intensities versus concentration of 4-ATP at 1074 cm^{-1} .

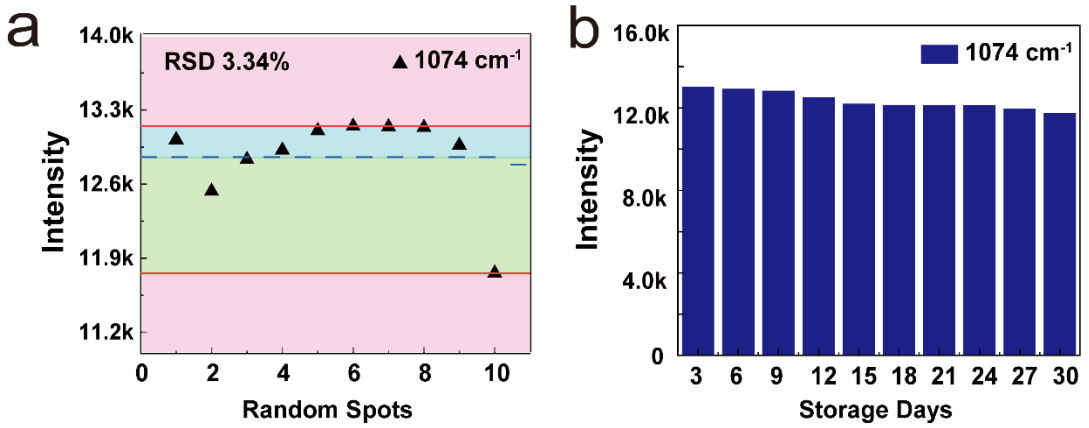

Fig. S10. (a) The corresponding SERS intensity distribution statistics of the 1074 cm^{-1} band. The average intensity is indicated by the blue line. (b) The relationships between SERS intensity at 1074 cm^{-1} of 10^{-7} M 4-ATP and the storage days.

S1. EF calculation.

According to the procedure outlined in earlier papers [1-2], the enhancement factor (EF) can be calculated from $EF=(I_{SERS}/N_{SERS})/(I_{Raman}/N_{Raman})$, where I_{SERS}, I_{Raman}, N_{SERS}, and N_{Raman} stand for, respectively, SERS intensity, Raman intensity, number of molecules being probed in SERS, and number of molecules being probed in Raman.

In this paper, the V_{SERS} are set as 3 μL, ensuring that the analytes are within the focus of the laser beam. The relative molecular mass of purchased 4-ATP is 155.17 g/mol. For the solid sample, the sampling volume is the product of the area of the laser spot (10 μm diameter) and the penetration depth (2 μm) of the focused laser beam. Assuming the density of bulk 4-ATP is 1.14 g cm^{-3} [3], N_{Raman} can be calculated to be 6.92×10^{11} ($N_{Raman}=1.14\ g/cm^{-3}\times\pi\times25\ \mu m^2\times2\ \mu m\times N_A/155.17\ g/mol=6.92\times10^{11}$).

In this paper, 3 μL of 10^{-7} M 4-ATP solution left a spot of ca.2.7 mm in diameter. N_{SERS} can be calculated to be 2.48×10^5 ($N_{SERS}=10^{-7}\ mol/L\times3\ \mu L\times N_A/(1.35\ mm)^2/\pi\times(25\ \mu m^2\times\pi)=2.48\times10^5$). In these Raman peaks, the maximum enhancement is observed at 1074 cm^{-1}, which was chosen to estimate the EF of SERS substrate according to the method previously reported. Since the ratio of I_{SERS} to I_{Raman} was approximately 23.4 (**Fig. S11**), EF was calculated to be $23.4\times(6.92\times10^{11}/2.48\times10^5)=6.53\times10^7$.

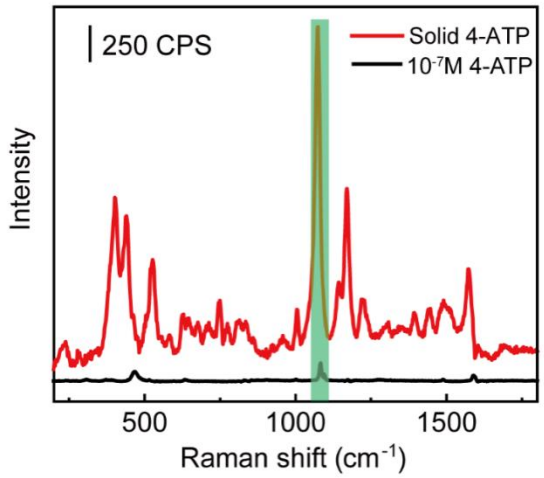

Fig. S11. SERS spectra of 10^{-7} M 4-ATP recorded on AuNP@UIO-66/Au, and the normal Raman spectra of solid 4-ATP.

S2. 2D Finite-difference time-domain (FDTD) simulation.

The electromagnetic field enhancement of AuNP@UIO-66/Au was simulated with the 2D-FDTD software (Lumerical, Canada). The structural parameters were set according to the acquired experimental data. The permittivity of AuNP was described by LorentzDrude model[4]:

A total-field scattered-field (TFSF) source propagating parallel to the Z-axis was applied with polarization along the X-axis and Y-axis to satisfy phase (Ex) = 0 and phase (Ey) = +90. Perfectly matched layers (PMLs) were adopted for the Z-axis[5]. The simulation region was a 320 × 260 × 260 nm^3 cuboid space surrounded by 12 absorber layers to avoid numerical reflections.

Table S1. The porosity analysis of the UIO-66 and AuNP@UIO-66/Au.

Samples	BET surface area (m^2/g)	Lagmuir surface area (m^2/g)	Total pore volume (ml/g)	Pore size (nm)
UIO-66	1232.9635	1795.6702	0.7115	1.1638
AuNP@UIO-66/Au	898.5733	1308.4256	1.1372	1.3503

Table S2. An overview on recently reported methods for 4-ATP determination.

Materials	LOD	EF	Ref.
AuNP@UIO-66/Au	1.1×10^{-11} M	6.53×10^{7}	this work
Ip_6@Au	1.0×10^{-7} M	-	6
SiO_2@Ag@SiO_2	1.0×10^{-7} M	-	7
Fe_3O_4@SiO_2-SO_3H@PPy@Au	1.0×10^{-6} M	4.9×10^{4}	8

Table S3. Corresponding band assignments of 4-AP, DHAB and 4-NP.[9]

SERS (cm^{-1})	Assignments
1110	ν (C-C)+β (C-H)
1146	ν (C-C)+β (C-N)
1335	ν (NO_2)
1382	ν (N-N)+ν (C-C)+β (C-H)
1441	ν (N-N)+ν (C-C)+β (C-H)
1488	ν (C-C)+β (C-H)
1576	ν (C-C)
1598	ν (C-C)

ν: stretching; β: in-plane bending

Table S4. An overview on recently reported methods for the reduction reaction.

Materials	Analytes	Amount of $NaBH_4$	Reaction Time	Ref
AuNP@UIO-66/Au	5 mM 4-NP	10 μM	10 min	this work
Au-m-Co_3O_4	0.5 mM 4-NP	0.2 M	5 min	10
PLAL-AuNPs/CeO_2-NTs	0.12 mM 4-NP	5 mM	20 min	11
AgNPs@GO/PET	10 mM 4-NP	1.0 M	20 min	12
Ag@AgCl	1 mM 4-NTP	0.1 M	14 min	13
Ag@AuNWs	5 mM 4-NTP	10 μM	20 min	14

Table S5. Corresponding band assignments of CV.[15]

SERS (cm^{-1}) of CV	SERS (cm^{-1}) of CV after the addition of H_2O_2	Assignments
416	416	γ (C^+-phenyl)
434	433	γ (Ph-C^+-Ph)
552	554	Ring skeletal vibration
719	718	γ (C-H)
794	797	Out-of-plane ring C-H
-	870	-
908	912	Ring skeletal vibration
936	--	Ring skeletal vibration
1172	1174	β (C-H)
1183	1191	ν (C-C)
1364	1366	ν (N-phenyl)
1437	1445	ν (C-C) + ring deformation
1532	1536	ν (N^+-phenyl)+ ν (C-C)
1583	1584	ν (C-C) + ν (C-C)
1615	1616	ν (C-C) + ν (C-N)

ν: stretching; β: bending in-plane; γ: bending out-of-plane

References

1 B. Fazio, C. D'Andrea, A. Foti, E. Messina, A. Irrera, M. G. Donato, V. Villari, N. Micali, O. M. Maragò and P. G. Gucciardi, *Scientific Reports,* **2016**, *6*, 26952.

2 E. C. Le Ru, E. Blackie, M. Meyer and P. G. Etchegoin, *The Journal of Physical Chemistry C,* **2007**, *111*, 13794-13803.

3 M. Jiang, Z. Qian, X. Zhou, X. Xin, J. Wu, C. Chen, G. Zhang, G. Xu and Y. Cheng, *PCCP,* **2015**, *17*, 21158-21163.

4 M. G. Blaber, M. D. Arnold and M. J. Ford, *The Journal of Physical Chemistry C,* **2009**, *113*, 3041-3045.

5 M. Su, C. Wang, T. Wang, Y. Jiang, Y. Xu and H. Liu, *Anal Chem,* **2020**, *92*, 6941-6948.

6 L. Zhang, Y. j. Weng, X. Liu, W. Gu, X. Zhang and L. Han, *Scientific Reports,* **2020**, *10*, 5752.

7 M. G. Cha, H.-M. Kim, Y.-L. Kang, M. Lee, H. Kang, J. Kim, X.-H. Pham, T. H. Kim, E. Hahm, Y.-S. Lee, D. H. Jeong and B.-H. Jun, *PLOS ONE,* **2017**, *12*, e0178651.

8 G. Ren, M. Shang, H. Zou and W. Wang, *Mater Chem Phys,* **2016**, *173*, 333-339.

9 M. Muniz-Miranda, *Applied Catalysis B: Environmental,* **2014**, *146*, 147-150.

10 S. Zhou, C. Liu, W. Jin, L. Pan, Q. Jiang, Y. Hu and Y. Kong, *ACS Applied Nano Materials,* **2021**, *4*, 4763-4773.

11 J. Zhang, G. Chen, M. Chaker, F. Rosei and D. Ma, *Applied Catalysis B: Environmental,* **2013**, *132-133*, 107-115.

12 K. Sharma, M. Ali, R. Singh, S. Majhi, S. Sharma, C. S. P. Tripathi and D. Guin, *J Phys Chem Solids,* **2022**, *165*, 110640.

13 Y. Lu, J. Mao, Z. Wang, Y. Qin and J. Zhou, *Catalysts,* **2020**, *10*, 746.

14 Y. Zhu, H. Tang, H. Wang and Y. Li, *Anal Chem,* **2021**, *93*, 11736-11744.

15 M. Vinod, K.G. Gopchandran, Progress in Natural Science: Materials International, **2014**, 24, 569–578.